Electronic Supplementary Material (ESI) for:

Hierarchically porous UiO-66 with tunable mesopores and oxygen vacancies for enhanced arsenic removal

Rongming Xu,[abc] Qinghua Ji,[a] Pin Zhao,[a] Meipeng Jian,[d] Chao Xiang,[a] Chengzhi Hu,*[c] Gong Zhang,[a] Chaochun Tang,[b] Ruiping Liu,[ce] Xiwang Zhang*[d] and Jiuhui Qu[ace]

[a] *Center for Water and Ecology, State Key Joint Laboratory of Environment Simulation and Pollution Control, School of Environment, Tsinghua University, Beijing 100085, China.*

[b] *School of Civil Engineering and Architecture, East China JiaoTong University, Nanchang 330013, Jiangxi, China.*

[c] *State Key Laboratory of Environmental Aquatic Chemistry, Research Center for Eco-Environmental Sciences, Chinese Academy of Sciences, Beijing 100085, China E-mail: czhu@rcees.ac.cn*

[d] *Department of Chemical Engineering, Monash University, Clayton, VIC 3800, Australia. E-mail: xiwang.zhang@monash.edu*

[e] *University of Chinese Academy of Sciences, Beijing 100049, China*

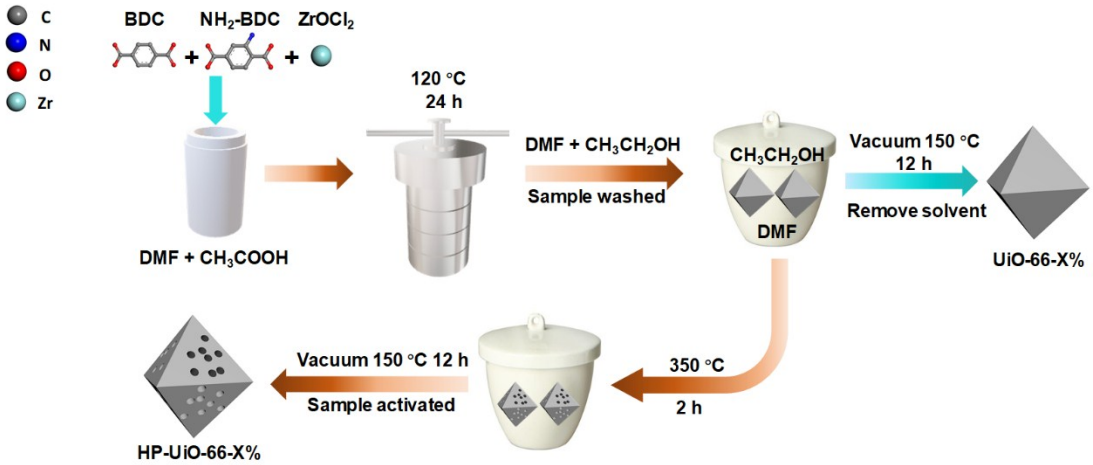

Fig. S1 Schematic diagram of UiO-66-X% and HP-UiO-66-X% synthesis process (X = 0, 5, 15, 30, 40).

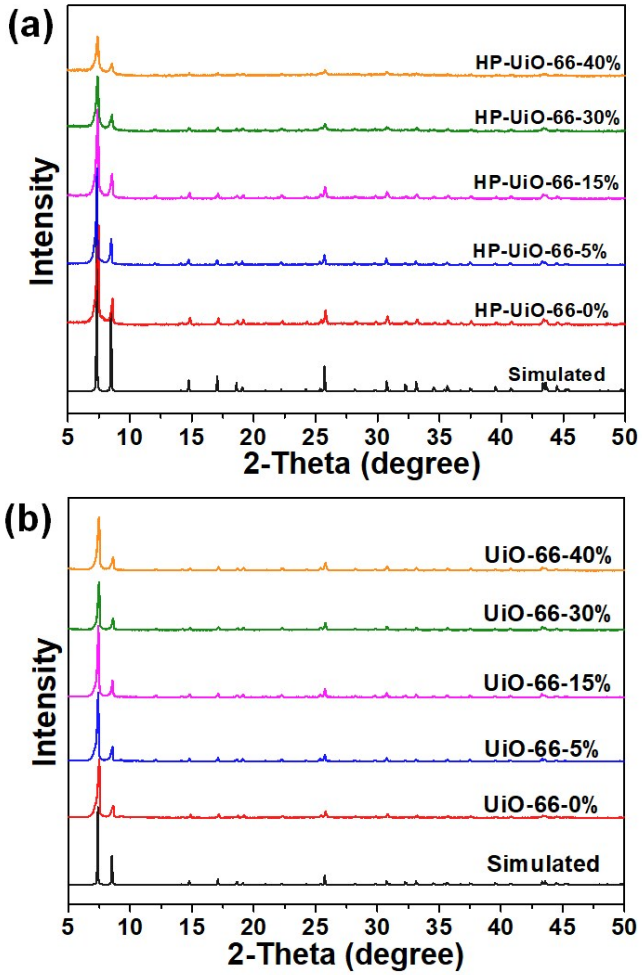

Fig. S2 Powder XRD patterns of (a) HP-UiO-66-X% and (b) UiO-66-X% (X = 0, 5, 15, 30, 40).

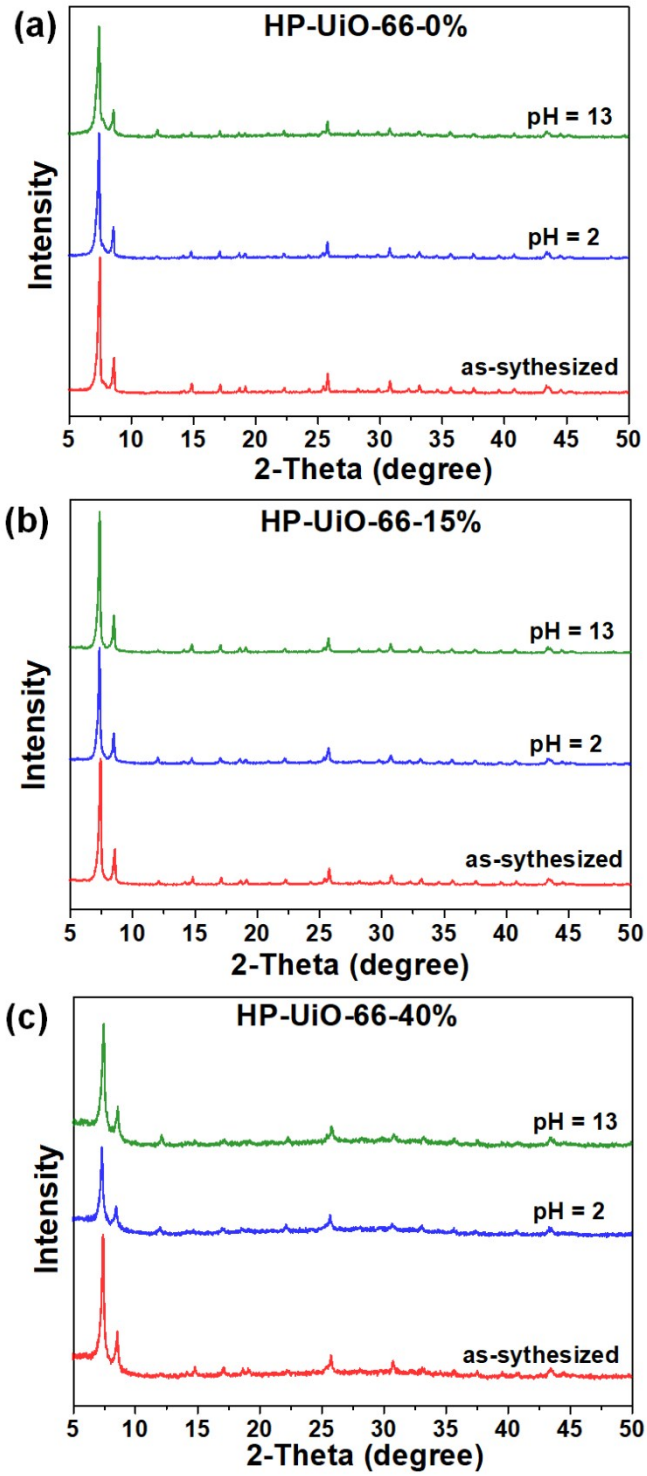

Fig. S3 Powder XRD patterns of (a) HP-UiO-66-0%, (b) HP-UiO-66-15%, (c) HP-UiO-66-40% before and after being treated in acidic and alkaline aqueous solutions for 48 h.

Table. S1 N_2 adsorption-desorption measurement results of HP-UiO-66-X% (X = 0, 5, 15, 30, 40).

HP-UiO-66-X%	BET Surface Area (m^2/g)	total pore volume (cm^3/g)	t-Plot micropore volume (cm^3/g)	Mesopore volume (cm^3/g)	Mesopore percentage (%)
0	826.05	0.4494	0.3426	0.1068	23.7
5	824.6	0.4521	0.3386	0.1135	25.1
15	800.23	0.5167	0.3062	0.2105	40.7
30	715.81	0.5093	0.2239	0.2854	56.0
40	574.07	0.4061	0.1583	0.2478	61.0

* $V_{Mesopore} = V_{Total\ pore} - V_{t\text{-}Plot\ micropore}$

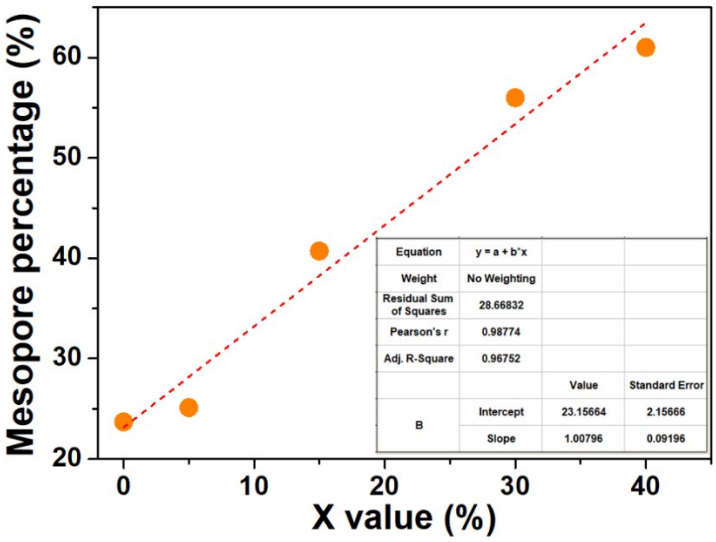

Fig. S4 The relationship of NH_2-BDC ligand concentration and mesopores percentage in HP-UiO-66-X%.

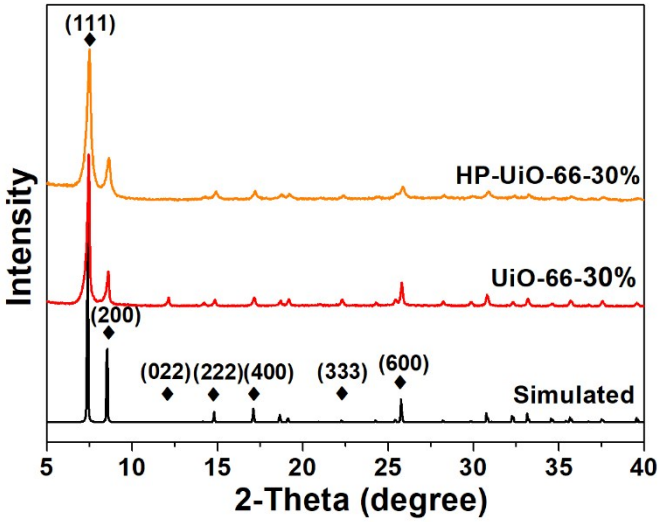

Fig. S5 Powder XRD patterns of UiO-66-30% and HP-UiO-66-30%.

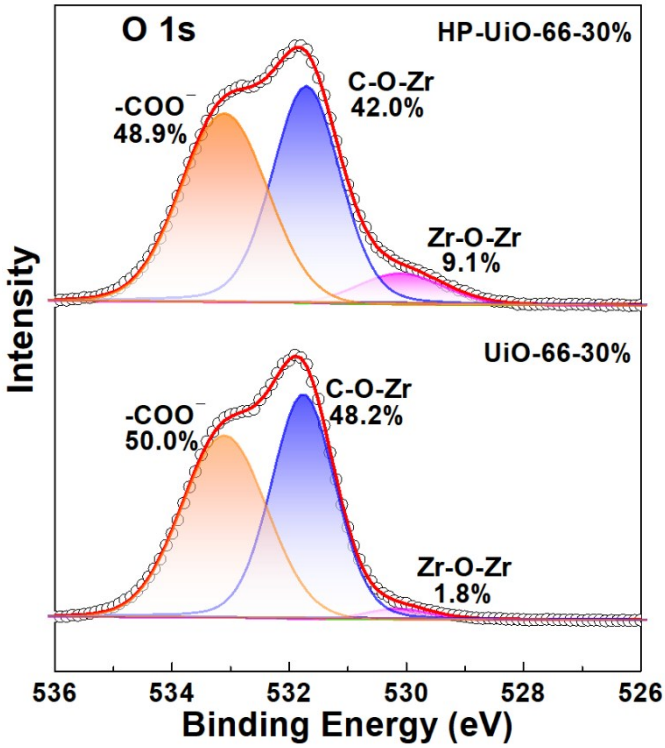

Fig. S6 O 1s High-resolution XPS spectra of UiO-66-30% and HP-UiO-66-30%.

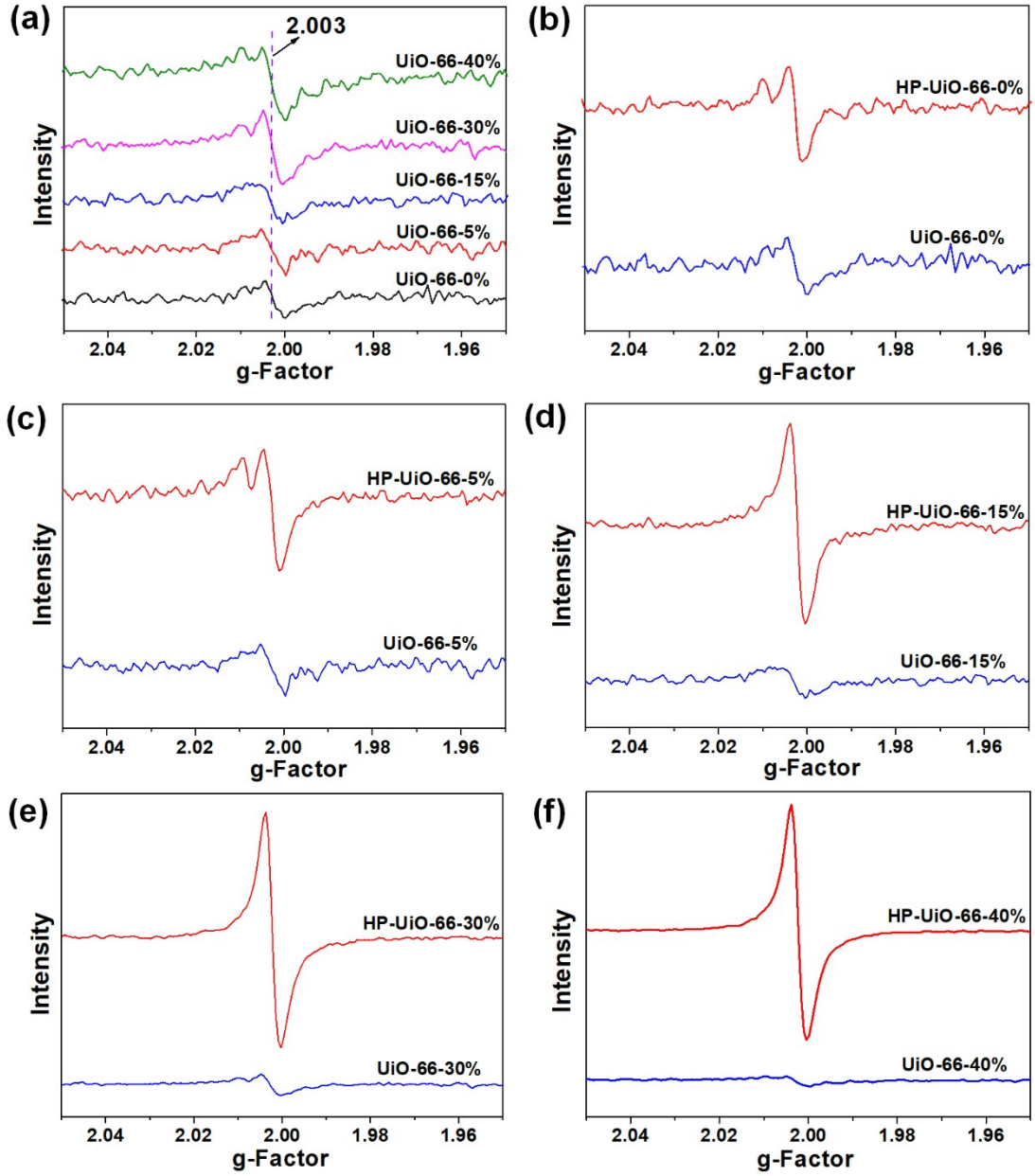

Fig. S7 (a) EPR spectra of UiO-66-X%, b-f) The comparison of EPR spectra between UiO-66-X% and HP-UiO-66-X% (X = 0, 5, 15, 30, 40). As the previously reported by H.L Jiang and coworkers,[1] the presence of a large amount of modulator (HOAc) would suppress the deprotonation of linkers and the replacement of modulators by linkers, resulting in more modulator residing on the Zr_6O_6 clusters and thus more defects in the obtained UiO-66-X%. Thus, there has some defects inherent to the UiO-66-X% structure (Fig. S7a). Visibly, when the content of thermolabile ligands increases to 15 %, the defects inherent to the UiO-66-X% can be negligible.

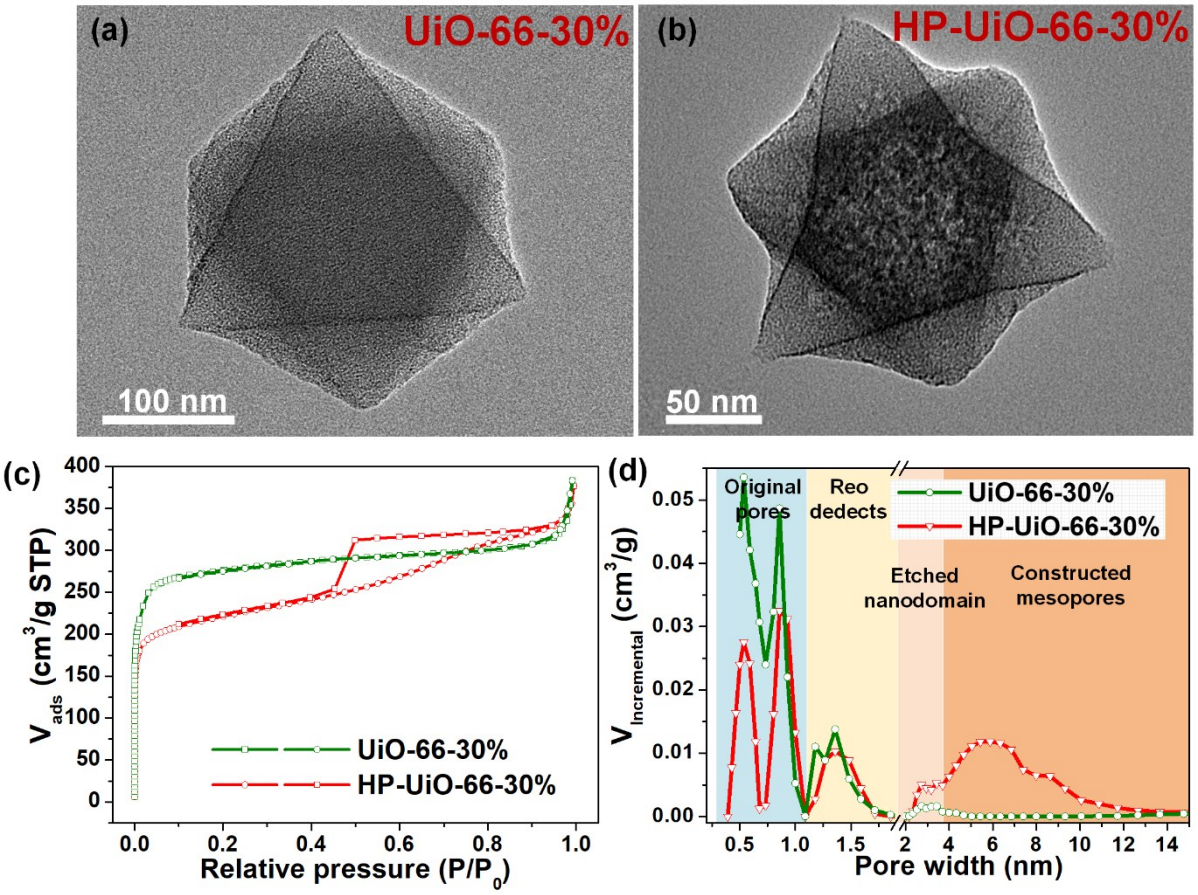

Fig. S8 TEM images of (a) UiO-66-30% and (b) HP-UiO-66-30%. (c) N_2 adsorption/desorption isotherms, (d) pore size distributions based on density-functional theory (DFT) analysis of UiO-66-30% and HP-UiO-66-30%. Particularly, the pore diameter of 1.1∼1.9 nm can be attributed to "Reo defects", which is very common in Zr-MOFs. While the small amount structural defects at range of 2~4 nm corresponding to "etched nanodomain".[2]

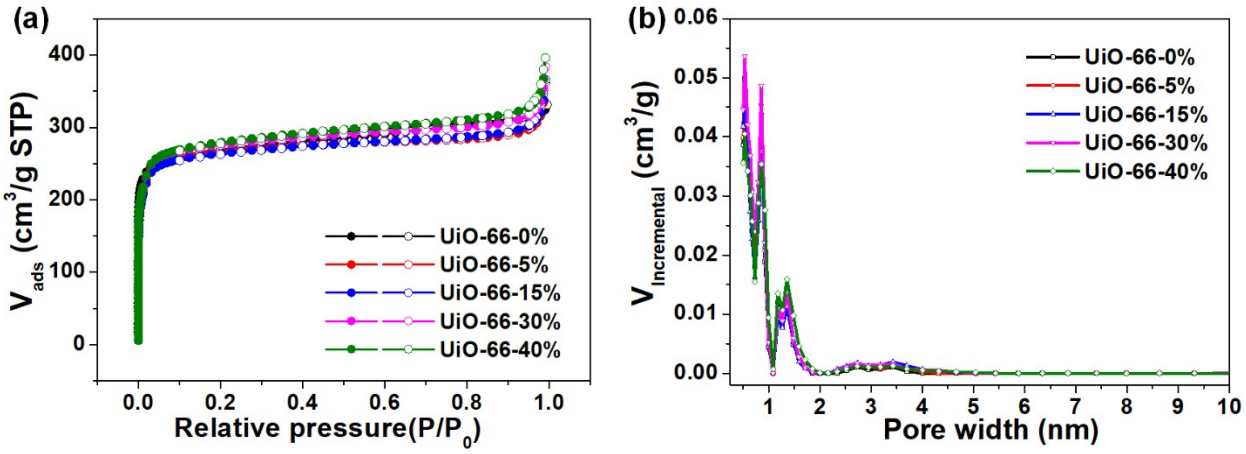

Fig. S9 (a) N_2 adsorption/desorption isotherms and (b) pore size distributions based on density-functional theory (DFT) analysis of UiO-66-X% (X = 0, 5, 15, 30, 40).

Table. S2 Weber-Morris model fitting parameters for As(V) adsorption.

HP-UiO-66-X%	Weber-Morris model					
	K_{i1} (mg/g ·min$^{0.5}$)	R^2	K_{i2} (mg/g ·min$^{0.5}$)	R^2	K_{i3} (mg/g ·min$^{0.5}$)	R^2
0	5.87	0.99	2.40	0.98	0.32	0.99
5	6.70	0.99	3.80	0.97	0.39	0.95
15	10.65	0.96	4.98	0.96	0.28	0.81
30	11.87	0.99	8.55	0.98	0.95	0.86
40	24.90	0.99	10.03	0.99	0.47	0.72

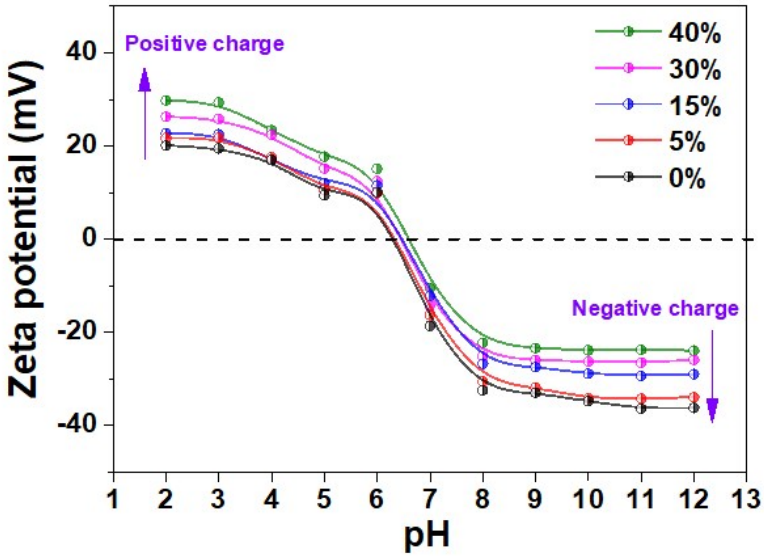

Fig. S10 Zeta potential curves of HP-UiO-66-X%.

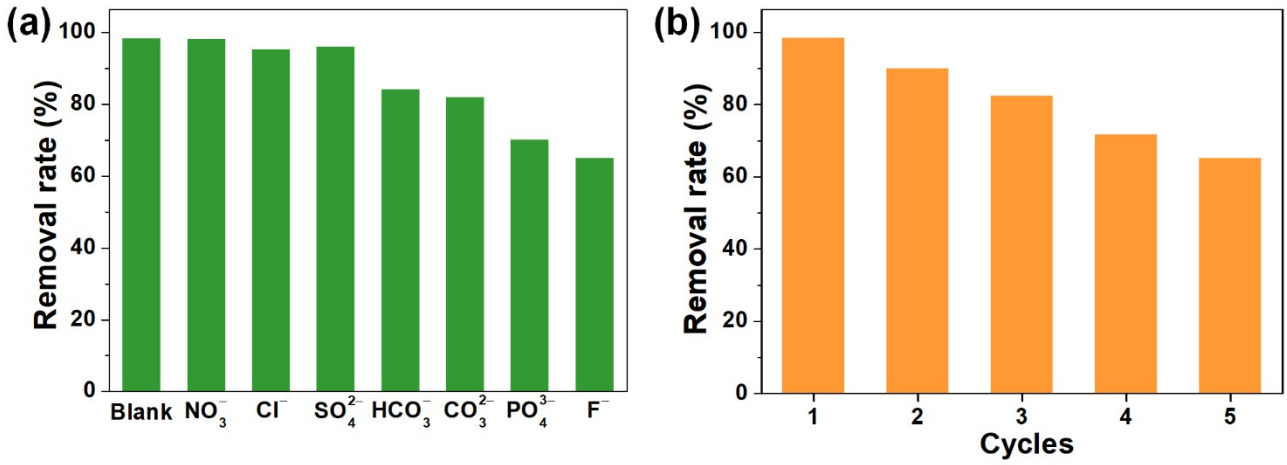

Fig. S11 (a) Influence of competitive anions on AsO_4^{3-} uptake by HP-UiO-66-40%. (b) HP-UiO-66-40% regeneration experiments .

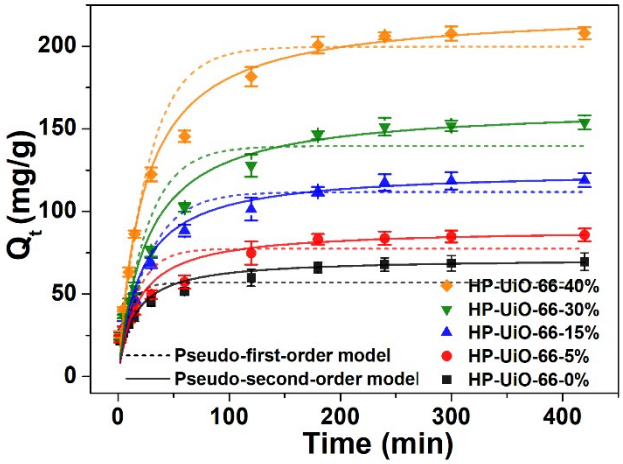

Fig. S12 Pseudo-first-order-and Pseudo-second-order kinetic model fitting curves for As(V) adsorption. (Experiment conditions, adsorbent dose: 50 mg/L, C_0: 20 mg/L, initial pH: 6, temperature: 25 °C)

Table. S3 Kinetic model fitting parameters for As(V) adsorption.

HP-UiO-66-X%	Pseudo-first-order model				Pseudo-second-order model		
	$Q_{e,\,exp}$ (mg/g)	K_1 (min^{-1})	$Q_{e,\,cal}$ (mg/g)	R^2	K_2 (g/mg·min)	$Q_{e,\,cal}$ (mg/g)	R^2
0	69.4	0.1072	56.79	0.731	9.9×10^{-4}	71.43	0.999
5	85.7	0.0597	77.30	0.794	6.3×10^{-4}	89.28	0.997
15	118.9	0.0376	111.66	0.930	3.9×10^{-4}	125.00	0.998
30	153.8	0.0397	139.54	0.904	2.3×10^{-4}	163.93	0.997
40	207.8	0.0377	199.64	0.975	1.9×10^{-4}	222.22	0.999

Table. S4 Isotherm model fitting parameters for As(V) adsorption.

HP-UiO-66-X%	Langmuir model			Freundlich model		
	Q_m (mg/g)	K_L (L/mg)	R^2	K_F (mg/g)	n	R^2
0	84.03	0.162	0.9976	19.42	2.95	0.9679
5	114.42	0.126	0.9935	21.10	2.57	0.9813
15	181.16	0.219	0.9972	36.40	2.45	0.9646
30	208.33	0.222	0.9954	41.85	2.43	0.9590
40	248.75	0.701	0.9932	72.23	2.71	0.9147

Table. S5 List of MOF-based materials for As(Ⅴ) removal.

Adsorbent	Suitable pH range	Experiment pH	Adsorption capacity (mg/g)	Ref.
HP-UiO-66-40%	2-13	6	248.75	This work
HP-UiO-66-30%	2-13	6	208.33	This work
Fe_3O_4@UiO-66	4-10	7	73.2	[3]
UiO-66	1-11	7	147.7	[4]
UiO-66-NH_2	3-10	7	76.9	[5]
UiO-66	3-10	7	85.0	[6]
UiO-67	5-9	7	105.0	[6]
Ethylenediamine-ZIF-8	4-11	7	83.5	[7]
Hierarchical ZIF-8	4-11	Unadjusted	90.92	[8]
ZIF-8	4-11	4	95.2	[9]
MnO_2@ZIF-8	4-11	7	60.0	[10]
ZIF-8	4-11	7	60.03	[11]
MIL-53(Fe)	3-10	5	21.27	[12]
MIL-53(Al)	2-10	5	105.6	[13]
MIL-88B(Fe)	2-10	6	156.7	[14]
NH_2-MIL-88(Fe)	3-11	6	125.0	[15]
MIL-88A	3-11	5	145.0	[16]
MIL-100(Fe)	Not given	7	110.0	[17]
α-Fe_2O_3@MIL-100(Fe)	Not given	3	181.8	[18]
Fe_3O_4@MIL-101(Cr)	Not given	7	80.0	[19]
MOF-74	3-10	6	130.0	[20]
MOF-808	Not given	4	24.8	[21]

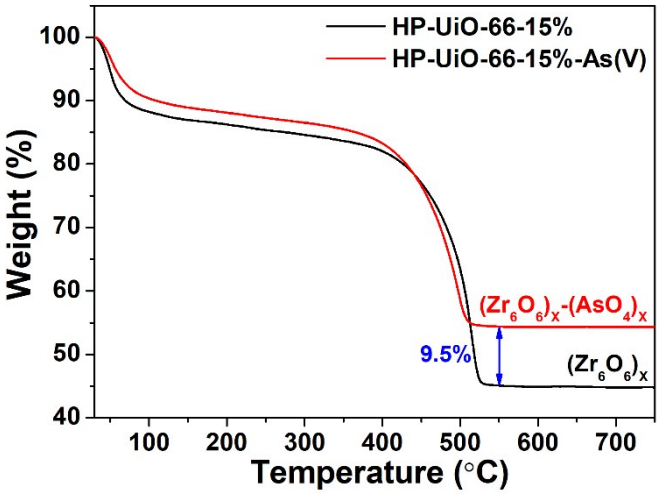

Fig. S13 Thermogravimetric analyses (TGA) of HP-UiO-66-15% and HP-UiO-66-15%-As(V). As shown in Fig. S13, the residual of HP-UiO-66-15% can be attributed to $(Zr_6O_6)_X$ cluster,[22] and the mass loss after thermal treatment was 55%. However, the mass loss of the sample after arsenic adsorption (HP-UiO-66-15%-As(V)) was 45.5%. The increase in the residual mass can be attributed to the arsenate coordinated to the zirconium atom. Thus, Zr–O–As(V) bond is a strong covalent bond. In addition, the pyrolysis temperature of the sample after arsenic adsorption shifted slightly to the left, indicating that the thermal stability of the adsorbent became worse.

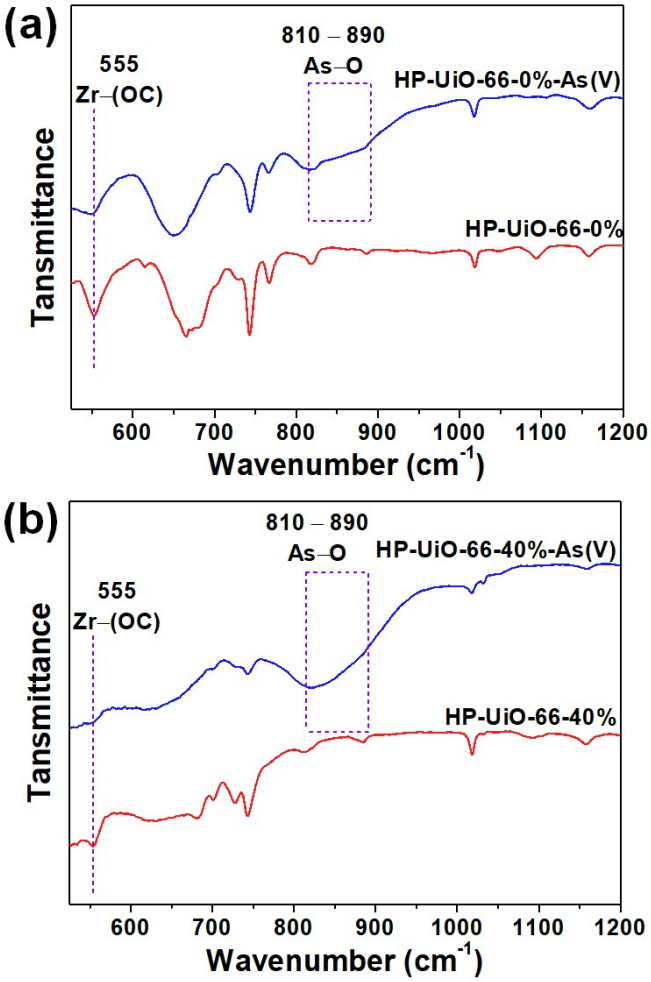

Fig. S14 FT-IR spectra of (a) HP-UiO-66-0%, (b) HP-UiO-66-40% before and after adsorption.

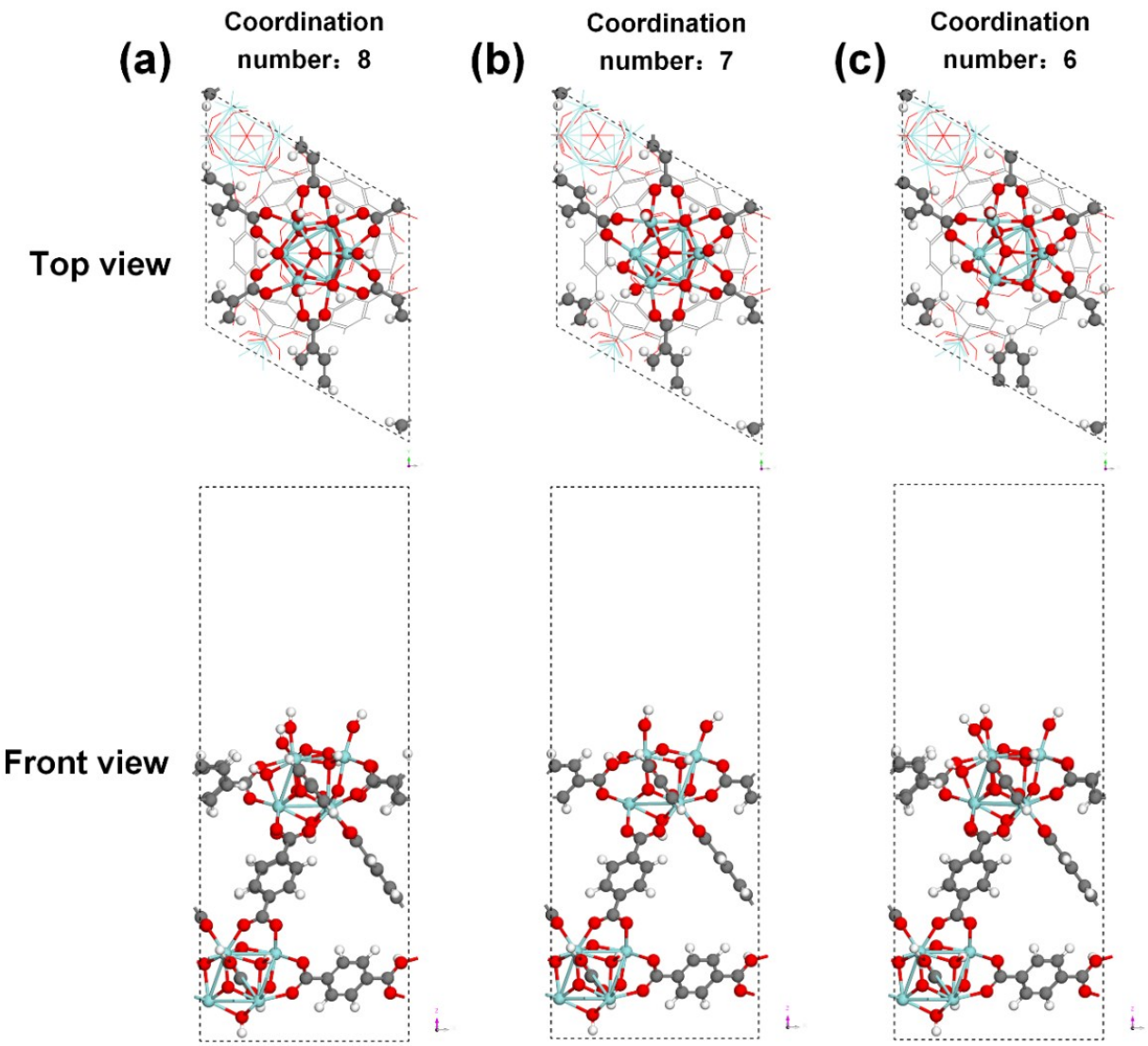

Fig. S15 Top and front view of optimized surface of UiO-66 with different zirconium coordination numbers. Decarboxylation changes the coordination number of zirconium atoms, leading to coordinatively unsaturated zirconium formation. Hence, we artificially removed the carboxyl group coordinated to the zirconium atom on UiO-66, thereby establishing the HP-UiO-66 model with coordinatively unsaturated zirconium atoms. Actually, when the hierarchically porous MOF (HP-UiO-66-X%) is placed in an aqueous solution, the open metal sites will be occupied by water molecules. But water molecules or hydroxyls can easily be replaced by arsenic. Thus, in order to simplify the calculation, we ignore this process.

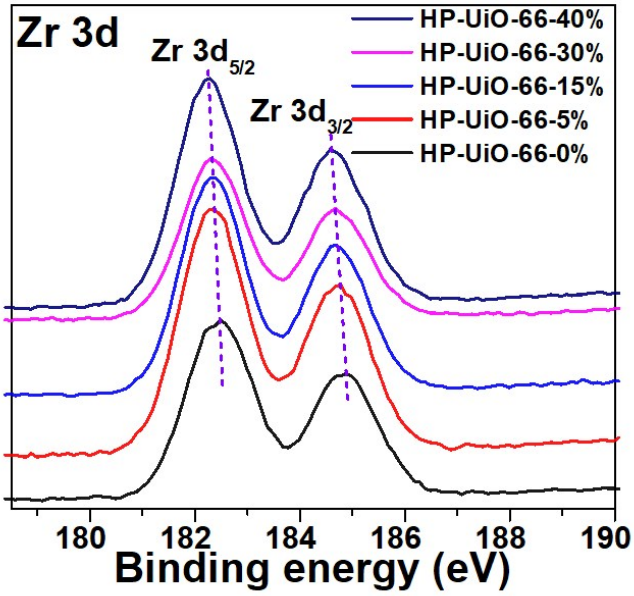

Fig. S16 High-resolution XPS spectra of Zr 3d in different HP-UiO-66-X% (X = 0, 5, 15, 30, 40). After decarboxylation, transferred electrons filling the d-band of Zr atoms, shifting the center of the band towards negative energy. The downshift of the d-band center reveals the d orbital energy of Zr atom is decreases. Zr 3d XPS spectra shifts to low binding energy direction as the NH_2-BDC ratio increases, indicating the free electrons transfer to Zr 3d orbital as the increase in the degree of decarboxylation, which is consistent with the d-band center downshift.

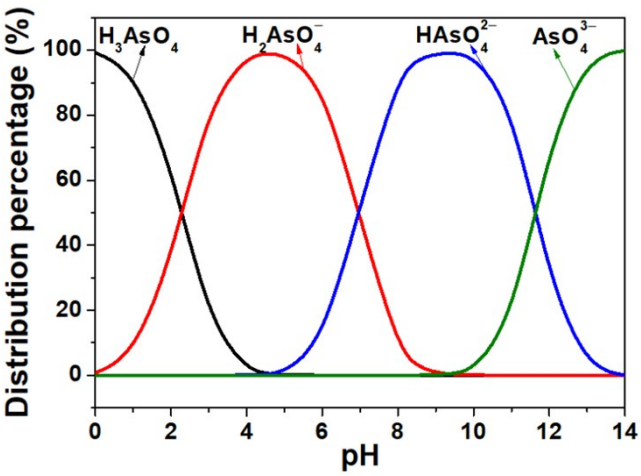

Fig. S17 As(V) relative distribution calculated by Visual MINTEQ simulation (C_0 = 20 mg/L).

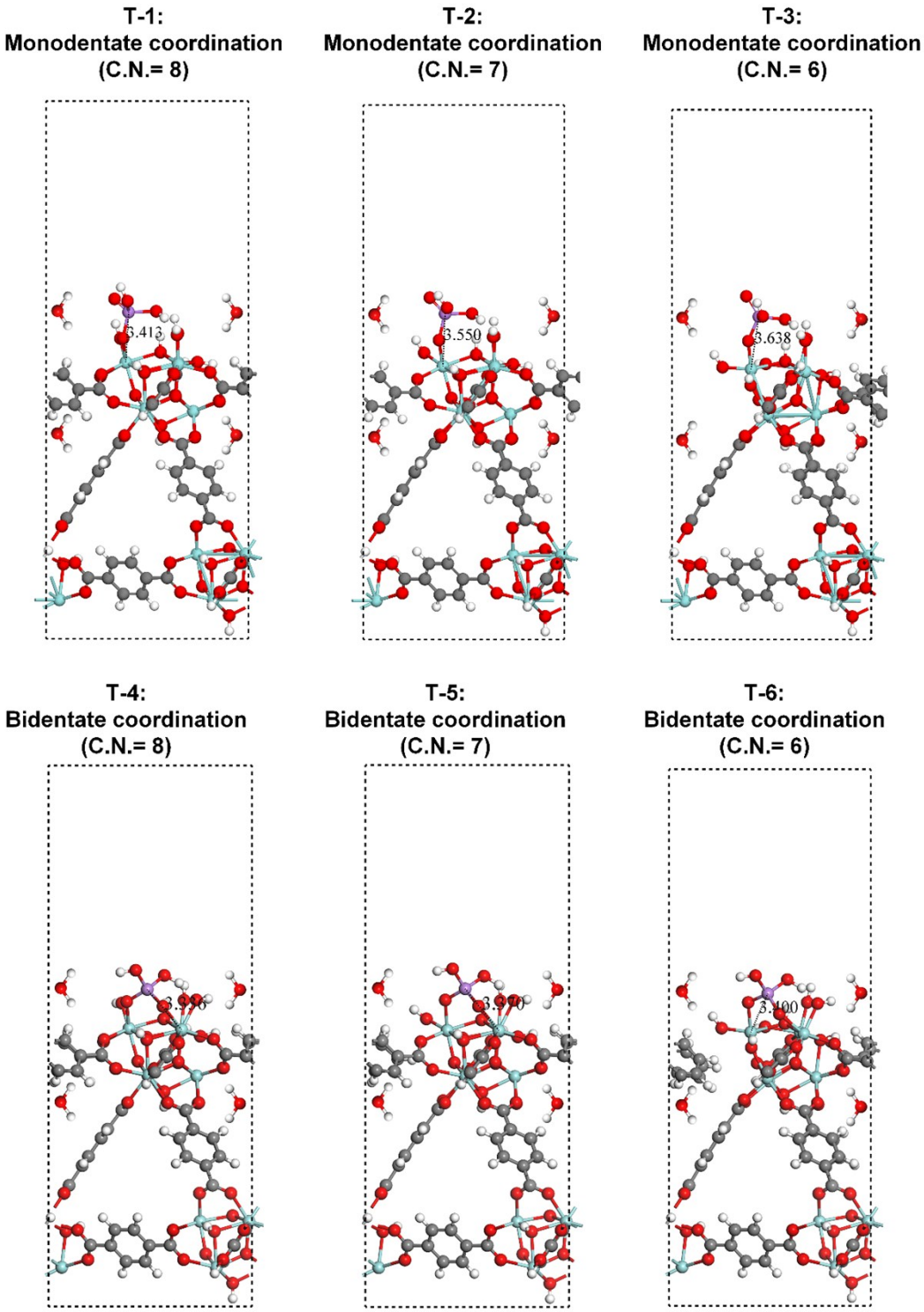

Fig. S18 Front view of optimized monodentate and bidentate coordination models of $H_2AsO_4^-$ on the surface of UiO-66 with different zirconium coordination numbers.

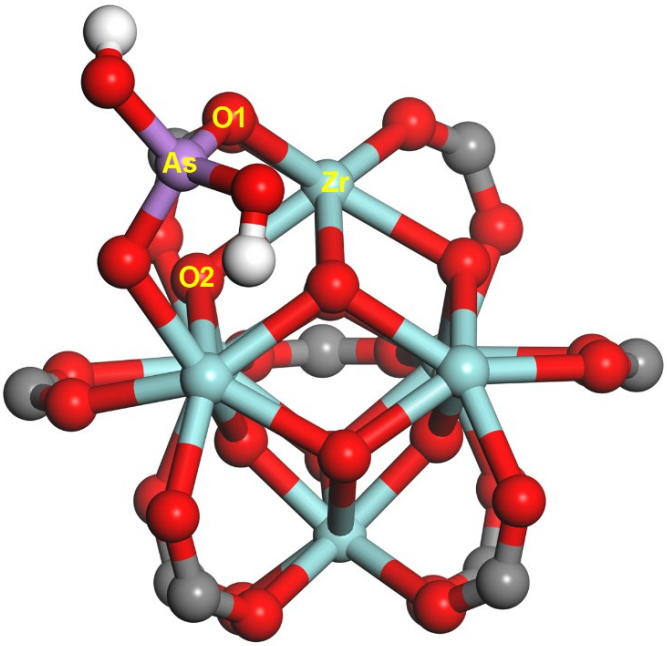

Fig. S19 Shell information of As atom.

Table. S6 The length of shell in the optimized coordination models by DFT calculations.

Model	Length of shell (Å)		
	As-O1	As-O2	As-Zr
T-1	1.714	3.045	3.413
T-2	1.719	3.529	3.550
T-3	1.723	3.490	3.638
T-4	1.691	3.073	3.552
T-5	1.697	2.996	3.471
T-6	1.705	2.887	3.400

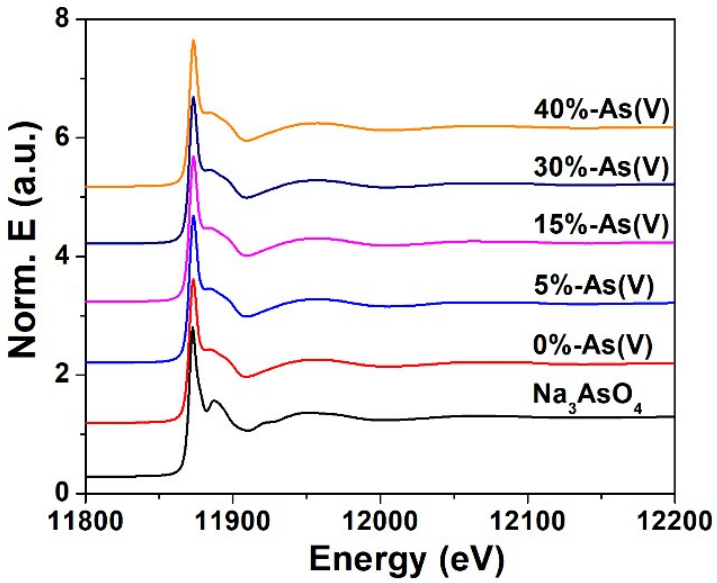

Fig. S20 Normalized As K-edge EXAFS spectra of Na_3AsO_4 and HP-UiO-66-X% after As(V) loaded.

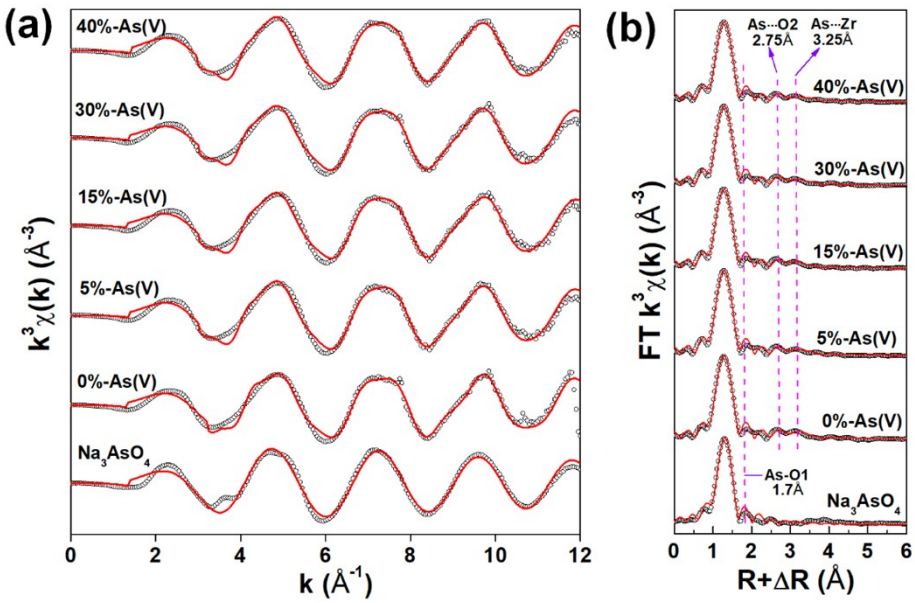

Fig. S21 Experimental (black circles) and fitted (red lines) (a) K^3-weighted As K-edge EXAFS spectra and (b) their corresponding magnitude part of Fourier transformed R-space.

Table. S7 EXAFS shell-fit results for As(V) adsorbed HP-UiO-66-X%.

Sample	Path	C.N.	R (Å)	$\sigma^2\times10^3$ (Å^2)	ΔE (eV)	R factor
Na_3AsO_4 std	As-O1	4	1.70±0.01	1.7±1.2	7.4±3.0	0.016
0%-As(V)	As-O1	3.7±0.5	1.69±0.01	1.4±1.3	6.9±3.3	0.017
	As-Zr	2.0±0.5	3.28±0.03	15.2±4.2	10.2±0.4	
5%-As(V)	As-O1	3.7±0.4	1.69±0.01	1.4±1.3	7.3±3.2	0.019
	As-Zr	2.1±1.0	3.25±0.04	12.7±8.7	15.4±0.6	
15%-As(V)	As-O1	3.7±0.4	1.69±0.01	1.3±1.2	6.9±3.2	0.018
	As-Zr	2.2±0.6	3.25±0.04	12.7±7.0	15.4±0.7	
30%-As(V)	As-O1	3.7±0.4	1.69±0.01	1.7±1.2	7.3±3.1	0.017
	As-Zr	2.1±0.8	3.24±0.04	12.8±5.7	15.4±0.6	
40%-As(V)	As-O1	3.7±0.4	1.69±0.01	1.3±1.2	7.8±2.9	0.017
	As-Zr	2.2±0.9	3.23±0.04	15.0±8.2	14.3±0.6	

As a result of O2 atom and As atom are isolated in the As-O2 path and the quality of oxygen atom is lighter, therefore, this path rank has low scores. Thus, if the path is added to the fitting process, the fitting will fail. However, although we can't obtain the data of the As-O2 path by fitting, it can be clearly seen in the Fourier transformed R-space spectra (Fig. S21b) that the length of As-O2 approximately 2.75 Å.

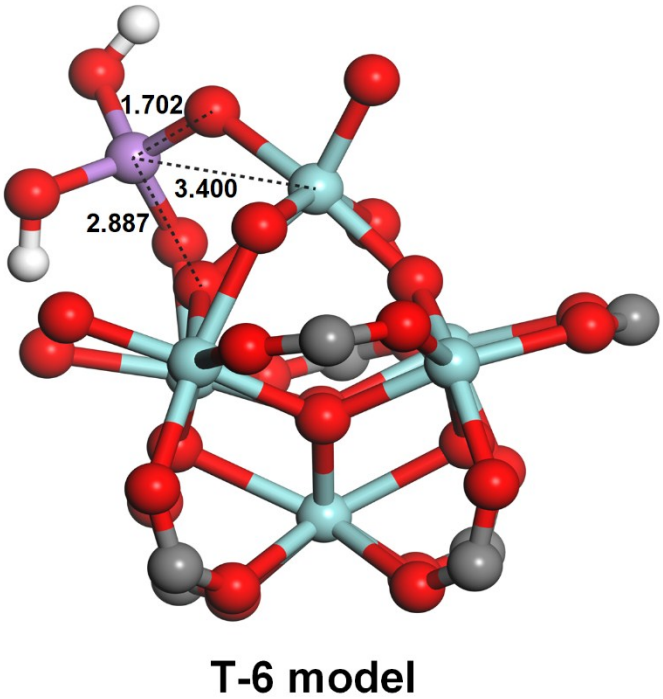

Fig. S22 The local coordination environment of $H_2AsO_4^-$ on the surface of HP-UiO-66-X%.

References

1 X. Ma, L. Wang, Q. Zhang, H. L. Jiang, *Angew. Chem.-Int. Edit.,* 2019, **58**, 12175-12179.

2 X. Q. Kong, H. X. Deng, F. Y. Yan, J. Kim, J. A. Swisher, B. Smit, O. M. Yaghi and J. A. Reimer, Science, 2013, 341, 882-885.

3 J.-B. Huo, L. Xu, X. Chen, Y. Zhang, J.-C. E. Yang, B. Yuan, M.-L. Fu, *Microporous Mesoporous Mat.,* 2019, **276**, 68-75.

4 C. Wang, X. Liu, J. P. Chen, K. Li, *Sci Rep,* 2015, **5**, 16613.

5 Z. W. Chang, Y. J. Lee, D. J. Lee, *J. Environ. Manage.,* 2019, **247**, 263-268.

6 C. O. Audu, H. G. T. Nguyen, C. Y. Chang, M. J. Katz, L. Mao, O. K. Farha, J. T. Hupp, S. T. Nguyen, *Chem. Sci.,* 2016, **7***,* 6492-6498.

7 M. Massoudinejad, M. Ghaderpoori, A. Shahsavani, A. Jafari, B. Kamarehie, A. Ghaderpoury, M. M. Amini, *J. Mol. Liq.,* 2018, **255**, 263-268.

8 Y.-n. Wu, M. Zhou, B. Zhang, B. Wu, J. Li, J. Qiao, X. Guan, F. Li, *Nanoscale,* 2014, **6**, 1105-1112.

9 J. Li, Y.-n. Wu, Z. Li, B. Zhang, M. Zhu, X. Hu, Y. Zhang, F. Li, *J. Phys. Chem. C,* 2014, **118**, 27382-27387.

10 M. Jian, H. Wang, R. Liu, J. Qu, H. Wang, X. Zhang, *Environ.-Sci. Nano,* 2016, **3**, 1186-1194.

11 M. Jian, B. Liu, G. Zhang, R. Liu, X. Zhang, *Colloid Surf. A-Physicochem. Eng. Asp.,* 2015, **465**, 67-76.

12 T. A. Vu, G. H. Le, C. D. Dao, L. Q. Dang, K. T. Nguyen, Q. K. Nguyen, P. T. Dang, H. T. K. Tran, Q. T. Duong, T. V. Nguyen, G. D. Lee, *RSC Adv.,* 2015, **5**, 5261-5268.

13 J. Li, Y. N. Wu, Z. Li, M. Zhu, F. Li, *Water Sci. Technol.,* 2014, **70**, 1391-1397.

14 S. Hou, Y. N. Wu, L. Feng, W. Chen, Y. Wang, C. Morlay, F. Li, *Dalton Trans.,* 2018, **47**, 2222-2231.

15 D. Xie, Y. Ma, Y. Gu, H. Zhou, H. Zhang, G. Wang, Y. Zhang, H. Zhao, *J. Mater. Chem. A,* 2017, **5**, 23794-23804.

16 H. Wu, M. D. Ma, W. Z. Gai, H. Yang, J. G. Zhou, Z. Cheng, P. Xu, Z. Y. Deng, *Environ. Sci. Pollut. Res.,* 2018, **25**, 27196-27202.

17 J. Cai, X. Wang, Y. Zhou, L. Jiang, C. Wang, *Phys. Chem. Chem. Phys.,* 2016, **18**, 10864-10867.

18 Z. Liu, J. Chen, Y. Wu, Y. Li, J. Zhao, P. Na, *J. Hazard. Mater.,* 2018, **343**, 304-314.

19 K. Folens, K. Leus, N. R. Nicomel, M. Meledina, S. Turner, G. Van Tendeloo, G. D. Laing, P. Van Der Voort, *Eur. J. Inorg. Chem.,* 2016, 4395-4401.

20 J. Sun, X. Zhang, A. Zhang, C. Liao, *J. Environ. Sci.,* 2019, **80**, 197-207.

21 Z.-Q. Li, J.-C. Yang, K.-W. Sui, N. Yin, *Mater. Lett.,* 2015, **160**, 412-414.

22 L. Feng, S. Yuan, L. L. Zhang, K. Tan, J. L. Li, A. Kirchon, L. M. Liu, P. Zhang, Y. Han, Y. J. Chabal and H. C. Zhou, *J. Am. Chem. Soc.*, 2018, **140**, 2363-2372.